AD-A116 331 TRW DEFENSE AND SPACE SYSTEMS GROUP REDONDO BEACH CA --ETC F/G 9/5
APPLICATIONS OF JOSEPHSON JUNCTION SQUIDS AND ARRAYS.(U)
APR 82 A H SILVER N00014-81-C-0615

UNCLASSIFIED NL

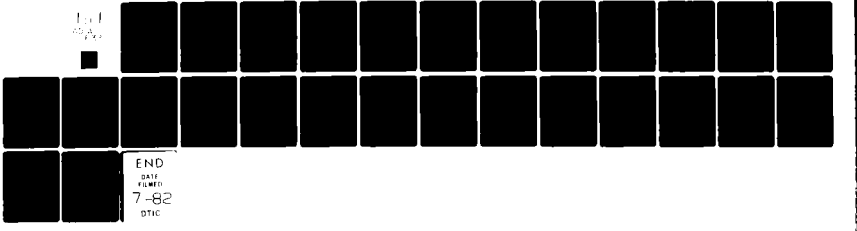

END
DATE FILMED
7-82
DTIC

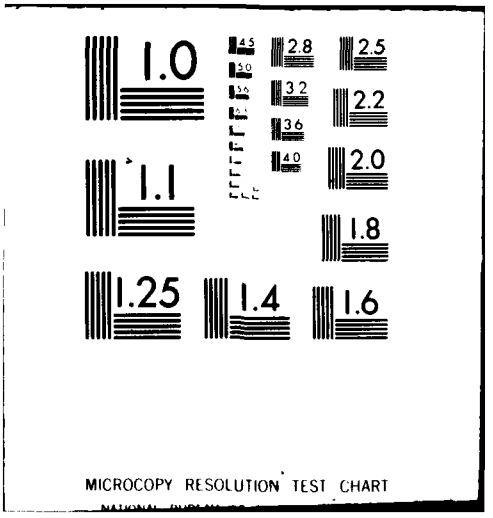
1.0
1.1
1.25
1.4
1.6
1.8
2.0
2.2
2.5
2.8
3.2
3.6
4.0
4.5
5.0
MICROCOPY RESOLUTION TEST CHART

(2)

SECOND QUARTERLY REPORT

TO THE

OFFICE OF NAVAL RESEARCH
CODE 414
800 N. QUINCY STREET
ARLINGTON, VA 22217

ON

APPLICATIONS OF JOSEPHSON JUNCTION SQUIDS AND ARRAYS

CONTRACT NO. N00014-81-C-0615

PREPARED BY

A.H. SILVER
ADVANCED PRODUCTS LABORATORY
APPLIED TECHNOLOGY DIVISION
TRW

30 April 1982

APPROVED FOR PUBLIC RELEASE; DISTRIBUTION UNLIMITED

I. INTRODUCTION

This is the second quarterly report for Contract No. N00014-81-C-0615, "Application of Josephson Junction SQUIDs and Arrays," covering the period from 2 January 1982 through 2 April 1982. The objectives of this program are to define and demonstrate applications of SQUIDs and SQUID arrays via analysis and experiment. The goals of this contract are to investigate and demonstrate the properties of a SQUID voltage-controlled-oscillator (VCO). These goals are being met by 1) analysis and simulation of a voltage-clamped resistive SQUID and a voltage-clamped dc SQUID, 2) design, fabrication and measurement of appropriate microwave matching transformer, and 3) design, fabrication and measurement of a SQUID VCO. We report on progress in these three areas.

A

2. ANALYSIS OF VOLTAGE-CLAMPED SQUIDS

We have investigated the voltage-clamped SQUID in two forms: the resistive SQUID of Figure 1 and the dual resistive SQUID with common voltage-biasing resistor which we call the voltage-clamped dc SQUID (Figure 2). To the best of our knowledge, the resistive SQUID incorporating the full RSJ model with appropriate capacitance has not been previously investigated and this was undertaken to predict the operating characteristics before final design and fabrication.

The circuit of Figure 1 is driven by a current I which produces a dc voltage across r when $|I|>i_c$. The induced oscillation produces a time-dependent voltage across the L,C,i_c,R combination. We envision R to be the load to which power is delivered. Hence, a determination of this voltage will determine the power delivered. This circuit obeys the relation

$$\dddot{\theta}+(\eta_R+\eta_r)\ddot{\theta}+(1+\eta_R\eta_r+\beta\cos\theta)\dot{\theta}+\eta_r\beta\sin\theta=\dot{\beta}_I+\eta_r\beta_I \qquad (1)$$

where θ is the junction phase

$$\eta_R = \sqrt{L/C}\,/R$$

$$\eta_r = r/\sqrt{L/C}$$

$$\beta = 2\pi L i_c/\phi_o$$

$$\beta_I = 2\pi L I/\phi_o$$

and time is measured in t/ω_o where $\omega_o^2=(LC)^{-1}$. The voltage across the junction and load resistor R is related to θ by the Josephson relation

$$V=\omega_o\phi_o\dot{\theta}/2\pi \quad . \qquad (2)$$

The last term on the right hand side of Eq. (1), $\eta_r\beta_I=2\pi rI/\phi_o\omega_o$, is approximately the expected Josephson frequency ω_J/ω_o for $I>>i_c$. This is actually equivalent to a voltage source (rI) in series with r; the actual dc voltage across the junction is somewhat lower than rI and must be determined by either direct measurement or calculation of $\langle\dot{\theta}\rangle$.

The simulations conducted here were carried out for selected values of η_r, η_R, β and β_l with $\dot{\beta}_l=0$. A number of interesting and unexpected results were obtained in numerical computation of $\theta(t)$ and $\dot{\theta}(t)$ and are reported here. The results are essentially independent of η_r for all reasonable values of interest and so $\eta_r=10^{-3}$ is used in all calculations reported here. This means that $I \simeq 10^3 i_c$ and, hence, $\beta_l \simeq 10^3$ at $\omega_J=\omega_o$. We also note that $\eta_R=Q^{-1}$, the loaded circuit quality factor.

The transient response is dominated by ω_o, Q and ω_J. Figure 3 shows the time evolution of θ and $\dot{\theta}$ for Q=1, β =1 and expected Josephson frequencies of $\omega_o/20$ and ω_o. In each case the turn-on transient is short (approximately Q/ω_o) and associated with shock excitation of the resonant LC circuit, and the fundamental frequency of the periodic response is $\simeq \omega_J$. The oscillation shape appears to be dominated by ω_o^{-1}. We point out that the periodicity in a smoothly stepped θ is 2π. If the Q is raised to 5, the transient response is longer and the resonance frequency becomes further involved with the oscillation. Figure 4 shows the response at Q=5, β =1 and expected $\omega_J/\omega_o \simeq 1.2$ and 1.5 For $\omega_J/\omega_o \simeq 1.2$ (β_l=1200), the response is anharmonic although clearly there is a strong component near $\omega_J/2\omega_o$ and ω_J/ω_o. At $\omega_J/\omega_o \simeq 1.5$ (β_l=1500), the response is periodic again with a strong subharmonic component evident in the time response. At $\omega_J/\omega_o \simeq 2$ (β_l=2000), the response appears to be totally at $\omega_o=\omega_J/2$, while for Q=1 there is no evident subharmonic response as shown in Figure 5. For those situations where the response is aperiodic or has strong components at other than ω_J, the time-dependence was computed over many hundreds of cycles to eliminate any transients in assessing the oscillator performance. Generally, for either large β or large Q, the response becomes very complex and even aperiodic. The values required are not 100's, but of the order of 5. Even for smaller values, peculiarities occur somewhere in the spectrum if $\beta \cdot Q \gtrsim 2$.

In order to classify and quantify these measurements we have computed the power spectrum for selected values of Q and β as a function of β_l. These were computed over 100 periods of the fundamental frequency of the oscillator after a long time lapse from turn on, approximately 10^3 cycles. The Fourier amplitudes, including the zero frequency or dc value of $\dot{\theta}$,

were calculated. The zero frequency amplitude was then compared to the fundamental frequency which was first calculated in establishing the time interval for the numerical integration. In those cases for which the fundamental frequency is the expected Josephson frequency, $\langle\dot{\theta}\rangle \equiv \omega_J$. Otherwise $\langle\dot{\theta}\rangle = \omega_J/n$, except for anharmonic cases for which no fundamental frequency was found. Since the Fourier analysis was performed by a Fourier series rather than a Fourier integral, no spectra were determined for anharmonic cases.

The power delivered to the load resistance R at any frequency is

$$P_i = V_i^2/R \tag{3}$$

where V_i is the Fourier amplitude of the voltage at that frequency. From Eq. (2),

$$V_i = \frac{\omega_o \phi_o \dot{\theta}_i}{2\pi} \tag{4}$$

and

$$P_i = \frac{\omega_o \phi_o^2 \dot{\theta}_i^2}{(2\pi)^2 QL} \tag{5}$$

The values directly computed are $(\dot{\theta}_i^2/Q)$ which must be multiplied by $[\omega_o \phi_o^2 / (2\pi)^2 L]$ to obtain power in physical units.

Figure 6 shows the dependence of the power delivered at ω_J for $\omega_J = \omega_o$ as a function of Q for $\beta = 1$. Notice that the power has a maximum near Q=3. The abrupt decrease above Q≈3 is presumably the Q^{-1} dependence of Eq. (5). The decrease at low Q reflects the loading of the SQUID and a strong decrease in $\dot{\theta}$. The maximum value of the power is approximately $1.124\ \omega_o \phi_o^2/(2\pi)^2 L$. For design values $\omega_o = 2 \times 9 \times 10^{10}$ and $L = 5 \times 10^{-12}$H, this corresponds to 12.9nW. However, as we have seen, values of Q>2 leads to some undesirable spectral response. Nevertheless, even for Q≈1, the power is not even diminished by a factor of 2 from the peak value.

Figure 7 shows a compilation of the computed powers of the Josephson oscillations as a function of Q for $\beta = 1$. In the lower Q regime up to 2, the spectra are well behaved except for a subharmonic response at $\omega_J = 1.2\omega_o$, Q=2. For Q>2, there is a very strong subharmonic response at

$\omega_J=2\omega_o$, and anharmonic response near $\omega_J=1.2\omega_o$, Q=5. At 2<Q<5, the region near $\omega_J=1.2\omega_o$ exhibits a subharmonic behavior which is not plotted. The long dashed line with negative slope illustrates the approximate rolloff of the spectral harmonic amplitudes, roughly one decade in power per octave. The harmonic response is not plotted for clarity.

The strong subharmonic response when $\omega_J=2\omega_o$ which occurs at such modest Q's as 2.5 suggests degenerate parametric oscillations such as those predicted in the SQUID parametric amplifier [Silver, et al., "Parametric Properties of SQUID Lattice Arrays," IEEE Trans. Magn., MAG-17, pp. 412-415 (1981)]. This is also suggestive of the period-doubling effects attributed to strange attractors which are reported to visit nonlinear systems such as Josephson junctions. However, we also observe other subharmonic responses for Q=5, β=1 which do not fall in the period-doubling class. An example of this is shown in Figure 8 for Q=5, β=1, and β_1=1100.

These non-period-doubling subharmonics and the nonharmonic response which occur in the general vicinity of $\omega_J=1.2\omega_o$ for Q=5, β=1 are without explanation at this time. A possible clue to this behavior may be in noting that the resonance frequency of the circuit which we have called $\omega_o=(LC)^{-\frac{1}{2}}$ is in fact a time-dependent quantity through the phase-dependent Josephson inductance. The effective circuit inductance is

$$L_{eff}^{-1} = L^{-1}\,(1+\beta\cos\theta)\ . \qquad (6)$$

and the resonance frequency varies as

$$\omega_r = \omega_o\,(1+\beta\cos\theta)^{\frac{1}{2}}\ . \qquad (7)$$

Over each period as $\theta=0\rightarrow 2\pi$, ω_r varies from $0\rightarrow\omega_o\sqrt{2}$ for β=1. Since the values near $\omega_r=0$ occur when $\theta=\pi$, the SQUID spends a relatively short time at these very low resonance frequencies and a correspondingly long time near $\omega_r=\sqrt{2}\omega_o$. Perhaps some interactions between the Josephson oscillations and the time-dependent resonant circuit induces the unexpected subharmonics and anharmonic behavior. We hope to explore this effect further during the next year.

The effect of increasing β at constant Q=1 is illustrated in the power spectra of Figure 9. The bold printed points are the Josephson frequencies and the lighter points connected by straight lines are the predicted harmonics. In order to preserve some clarity, not all harmonic spectra are shown. Below β=3.14, all computed points are well behaved with some expected harmonics but no subharmonic response. For β=3.14, we observe subharmonics as we did for large Q values at β=1. At even larger β-values, the time dependent response becomes even more complex and we have not computed spectral powers. Such β-values would be considered outside the normal range for a SQUID. We report these effects and point out that increasing β moves toward the non-SQUID Josephson junction for which this analysis indicates very poor quality VCO.

3. VOLTAGE-CLAMPED DC SQUID

We have carried out some preliminary simulations of the voltage-clamped dc SQUID as shown in Figure 2. The two coupled equations which describe this device are

$$\dddot{\theta}_+ + (\eta_R+2\eta_r)\ddot{\theta}_+ + [1+2\eta_R\eta_r + \frac{\beta}{2}\cos(\theta_++\theta_-) + \frac{\beta}{2}\cos(\theta_+-\theta_-)]\dot{\theta}_+ +$$

$$[\frac{\beta}{2}\cos(\theta_++\theta_-) - \frac{\beta}{2}\cos(\theta_+-\theta_-)]\dot{\theta}_- + \eta_r\beta\sin(\theta_++\theta_-) + \eta_r\beta\sin(\theta_+-\theta_-) = \eta_r\beta_o \quad (8)$$

and

$$\ddot{\theta}_- + \eta_R\dot{\theta}_- + \frac{\beta}{2}\sin(\theta_++\theta_-) - \frac{\beta}{2}\sin(\theta_+-\theta_-) + \theta_- = \beta_1 \quad (9)$$

where $\beta_o = 2\pi LI_o/\phi_o$, $\beta_1 = 2\pi LI_1/\phi_o$, $\theta_+ = \frac{\theta_R+\theta_L}{2}$ and $\theta_- = \frac{\theta_R-\theta_L}{2}$.

θ_R and θ_L refer to the phases of the right and left hand junctions, respectively, and we have defined β as $2\pi LI_c/\phi_o$, where L is the inductance of one-half of the dc SQUID. In a limited number of simulations with $\beta=1$ and $\beta_1=0$, the dc SQUID behaves identically to the resistive rf SQUID with $\theta_-=\dot{\theta}_-=0$. The two junctions switch in-phase with one another and the resulting currents in L add in the small resistance r. For $\beta_1=\pi/2$ and $\beta=1$, the computation shows that $\dot{\theta}_-$ responds at the expected Josephson frequency while $\dot{\theta}_+$ responds at the second harmonic. This frequency doubling is a result of the alternate switching of the two junctions in each Josephson period. Figure 10 shows the time dependence of the various phases for $\eta_r=10^{-3}$, $\eta_R=Q_R^{-1}=1$, $\beta=1$, $\beta_1=\pi/2$ and $\beta_o=10^3$.

4. VCO DESIGN

The design of the VCO circuits have been completed. The resistive SQUID is placed at the low impedance end of the 50Ω to 1Ω transformer previously designed and reported. Connection to the transformer is with 1Ω microstrip. Two devices will be fabricated on each 1 cm x 2 cm silicon chip, with 4 chips on each 2" wafer.

Because of the predicted response discussed in Section 2, four different designs are employed to test the effects of Q and L on the power output and frequency response. The basic design is to choose L in order to set the flux quantum energy, $\phi_o^2/2L$, at a sufficiently large value. Then set $\beta=2\pi Li_c/\phi_o=1$, which fixes i_c. Setting $\omega_o^2=(LC)^{-1}$ to the operating frequency tunes the SQUID and selects C. If the Josephson plasma resonance is set equal to ω_o, then the Josephson current density is chosen. For the VCO, we assume that the load resistance dominates over any internal damping. With the previously designed transformer, this value should be 1Ω.

The initial design for the VCO was L=5pH, $\beta=1$, $\omega_o=2\pi x9x10^{10}$Hz, which for a 1Ω load produces a loaded Q=3.3. Because of the predicted effects for Q>2, we have designed four VCO's as follows:

VCO 1 L=5pH , C=65pF , Q=3.3 , i_c=67μA

VCO 2 L=10pH , 2C , Q=1.7 , $2i_c$

VCO 3 L=5pH, C , Q=1.7 , i_c
load with additional 1Ω resistance

VCO 4 L=2.5pH, 2C , Q=1.7 , $2i_c$
load with additional 0.25Ω resistance

Although a substantial amount of microwave power will be lost in the additional damping resistances, the last two VCO's will be devices damped to a low Q over essentially all frequencies, whereas the damping provided by the transformer in designs 1 and 2 is only well defined over a few GHz near resonance. A comparison of 2 and 3 will be particularly instructive. Figure 11 shows a composite printout of the seven masks designed for the VCO wafer.

5. IMPEDANCE TRANSFORMER

Work has continued on the impedance and dimensional transformer to couple the SQUID to a 50Ω line. In the last report, we reported on the electrical and geometrical design of the transformer, including the computer generated prediction of the VSWR and a composite drawing of three different test transformers. During this reporting period, the photolithographic masks were produced and a number of test transformers fabricated and measured.

The transformers were fabricated in a 1 cm x 2 cm format on 2" diameter silicon wafers with an insulating SiO_2 surface. Three test chips are produced on each wafer. Following fabrication, the wafer is cleaved with a modified Tempress scriber and the chips mounted in a holder suitable for connection to an OSM coaxial bulkhead launcher. Measurements are made at T=4K with an HP-8410 Network Analyzer. The data are in the form of the scattering matrix coefficients S_{11} and S_{12}. Only the magnitude of S is reported since the phase is difficult to calibrate with long coaxial lines into the helium dewar.

Figure 5 of the last quarterly report (15 January 1982) shows three different test transformer chips. These are mounted with a coaxial connector at each end as shown in Figure 12. As anticipated, connecting the coplanar input to the bulkhead connector was a significant problem. An acceptable solution is to use In solder to connect gold ribbon from the connector centerpin and bulkhead to the coplanar lines. To facilitate soldering to the Nb film, a gold film is evaporated over the Nb. This is done before the Nb is patterned. Figure 13 shows the response of the simple tapered coplanar lines at 4 kelvin; Figure 14 the response of the double-ended transformer, in which the 50Ω coplanar line is transformed to 1Ω microstrip at the center of the chip, and then transformed back to 50Ω coplanar at the other end of the chip. We have thus far not measured good S-parameter characteristics with the terminated transformers and we attribute this to a problem in making good contact with the resistors. In fact, the measured dc resistances are extremely high.

One problem which we discovered with the changeover from sapphire to silicon is associated with holding the wafer during ion-milling and oxidation. Since the silicon is more fragile than sapphire, one commonly resorts to using vacuum grease on the back side to hold the wafer to a heat sink and in tilted/inverted positions. We believe that the cleaning steps in removing the vacuum grease caused contamination of the front surface, particularly affecting the nature of contacts and junction formation. We also suffered a failure in our film thickness monitor which complicated our diagnostic experiments. These problems appear to have been resolved for now in that we are successfully fabricating junctions again. Tests of film contact resistance, which we believe is the problem with the terminated transformer, have not been completed.

6. PUBLICATIONS

We propose to submit a paper to the 1982 Applied Superconductivity Conference entitled "SQUID Voltage-Controlled-Oscillator," A copy of the proposed abstract is attached here. This paper will report on the analysis of the resistive SQUID and on the measurement which are anticipated in the near future. The Conference is November 30 - December 3, 1982.

SQUID VOLTAGE-CONTROLLED-OSCILLATOR,* A.H. Silver, R.D. Sandell and J.Z. Wilcox, TRW -- The microwave oscillator is an application of the Josephson junction which has eluded successful development since the earliest research on the Josephson effect. We have investigated the SQUID as a voltage-controlled source of microwave radiation. The low impedance "resistive" SQUID can be a relatively high power (≈ nW), tunable and monochromatic source of microwaves. Studies of the time-dependent junction phase and the available power spectrum as they vary with such device parameters as the loaded Q and SQUID $\beta \approx 2\pi Li_c/\phi_o$ not only exposes regions of degenerate parametric oscillations and chaotic instabilities, but also establishes the design rule for a well behaved oscillator, $Q\beta \approx 2$. Devices are fabricated in an integrated circuit format with a monolithic matching network centered at 9 GHz. Methods of further increasing power and impedance by combining SQUID have been investigated, particularly the voltage-clamped dc SQUID.

* Supported in part by Office of Naval Research Contract No. N00014-81-C-0615.

1. Category 8.
2. Arnold H. Silver, Mail Stop R1/1086, TRW, One Space Park, Redondo Beach, CA 90278; 213/535-2500.
3. A.H. Silver, R.D. Sandell, J.Z. Wilcox.
4. No Preference.

7. FINANCIAL

As of 2 April 1982 we have a total booked cost of $42,273 against a contract cost of $69,055 and fixed fee of $5,945. We anticipate completing the technical work by 31 July with an expenditure of $67,000. $2,055 is budgeted for completing the FINAL REPORT in August.

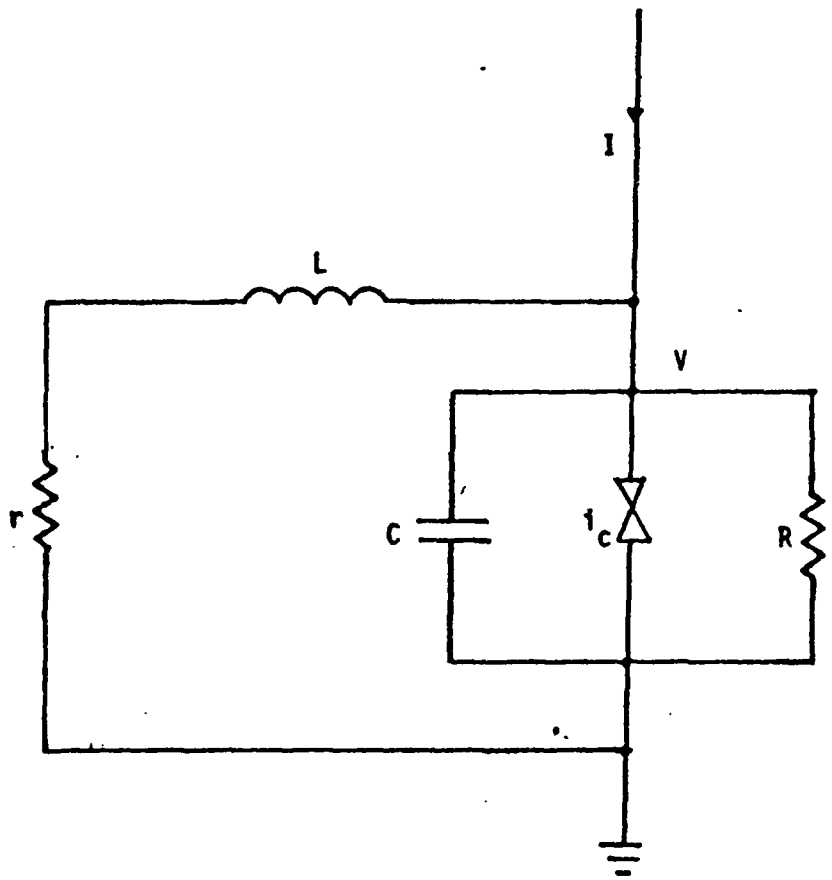

Figure 1. Equivalent circuit of the resistive SQUID VCO. The bias current is much greater than the junction current, i_c, and the bias resistance is much smaller than the load resistance R.

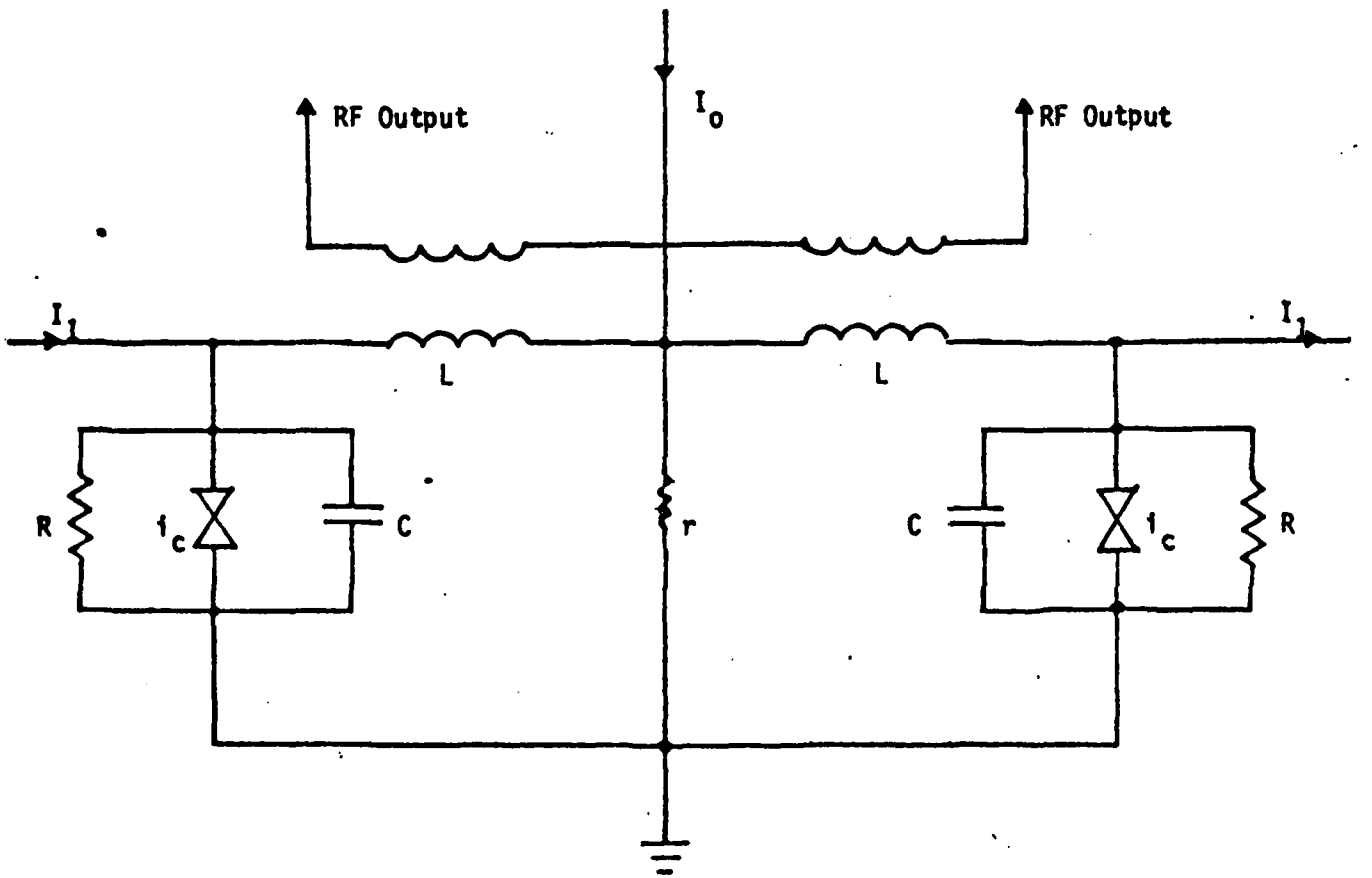

Figure 2. Equivalent circuit of the voltage-clamped dc SQUID with a summing output transformer. Comparison with Fig. 2 shows that this is equivalent to a pair of resistive SQUIDs with a common bias resistor.

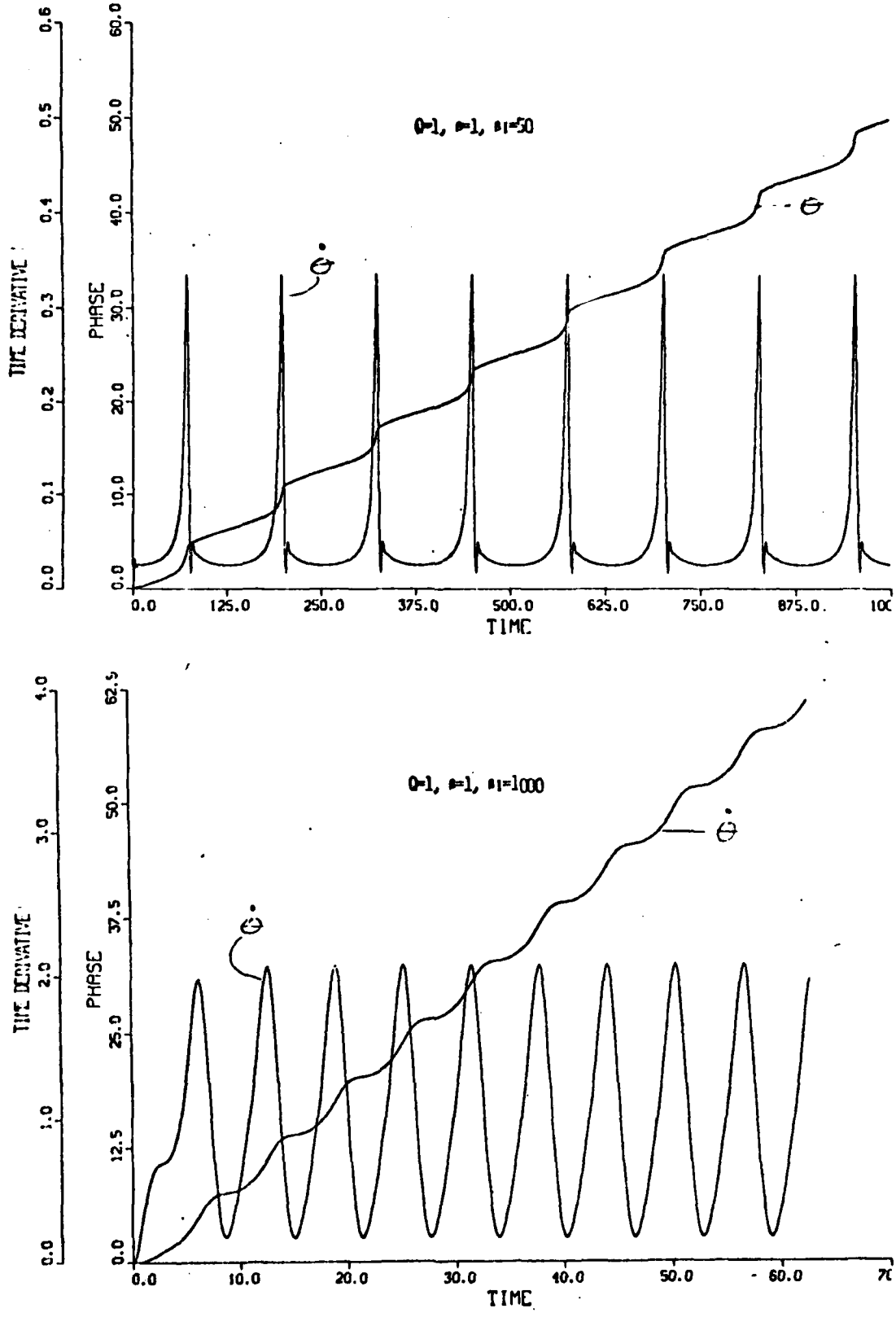

FIGURE 3. Computed time dependence of θ and $\dot{\theta}$ of the resistive SQUID for $Q=1$, $\beta=1$ and $\beta_1=50, 1000$ corresponding to $\omega_J/\omega_p \approx 0.05$ and 1, respectively. Time is measured in ω_p^{-1}.

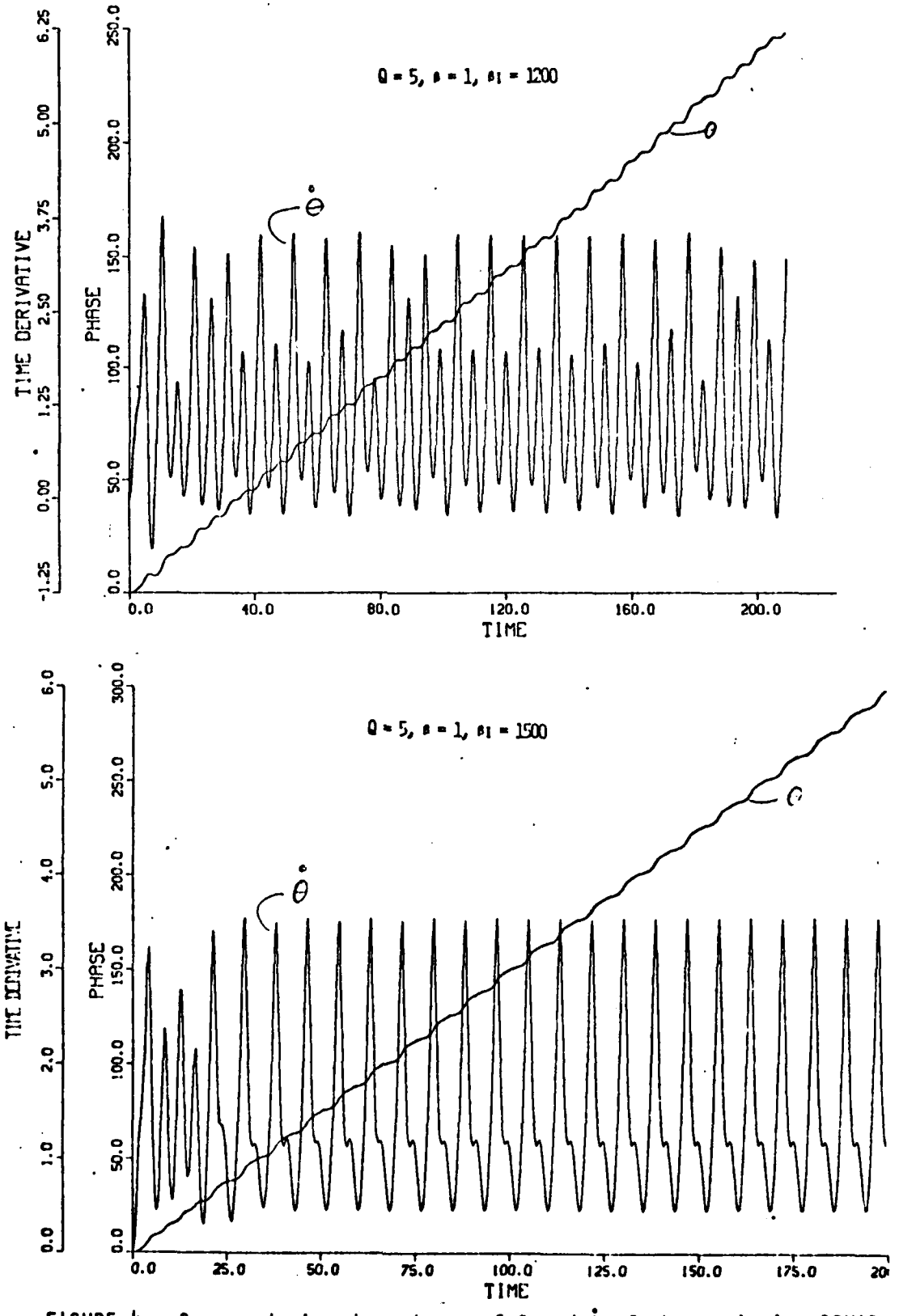

FIGURE 4. Computed time dependence of θ and $\dot{\theta}$ of the resistive SQUID for $Q=5$, $\beta=1$, and $\beta_1=1200$ and 1500 corresponding to $\omega_J/\omega_o=1.2$ and 1.5, respectively. Time is measured in ω_o^{-1}.

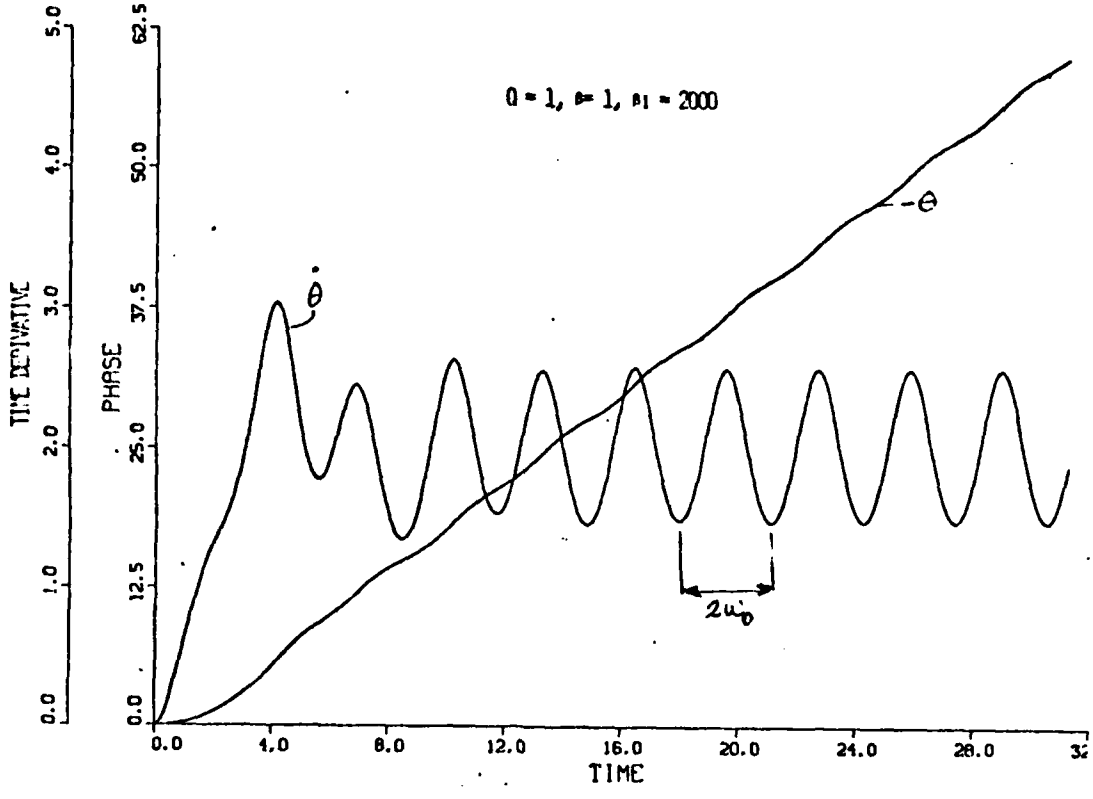

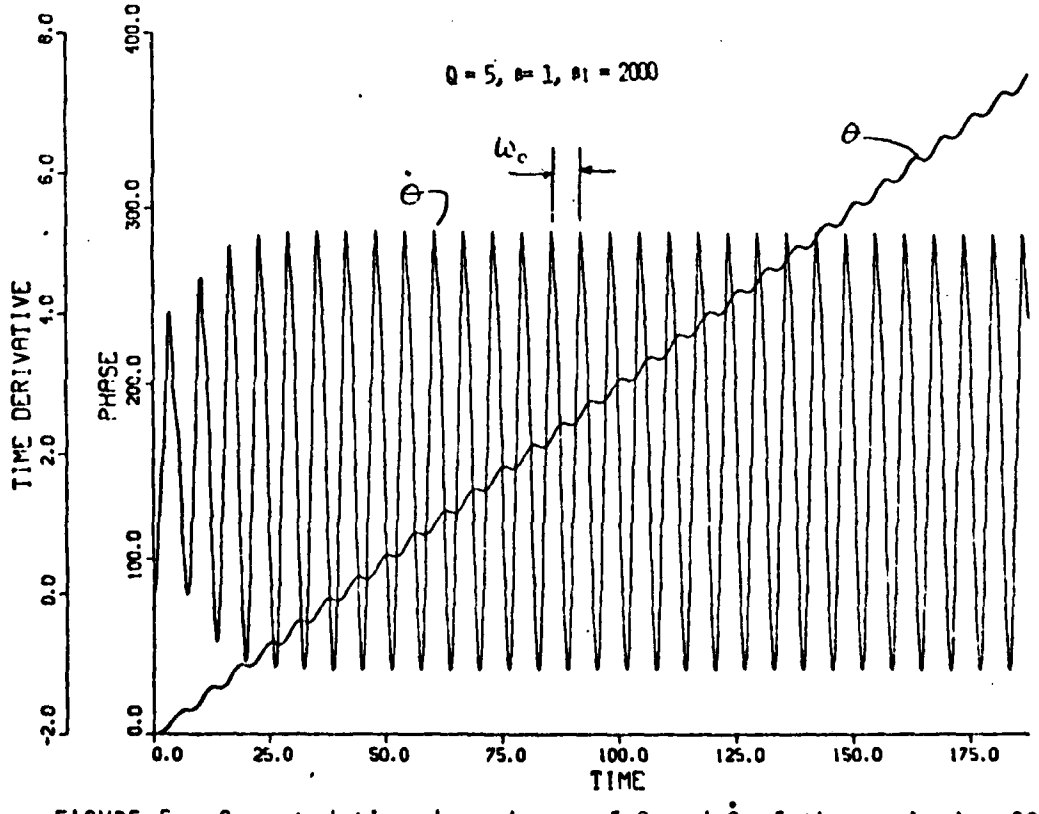

FIGURE 5. Computed time dependence of θ and $\dot{\theta}$ of the resistive SQUID for $\beta=1$, $\beta_1=2000$ and $Q=1,5$. This corresponds to $\omega_J=2\omega_0$. Time is measured in ω_0^{-1}.

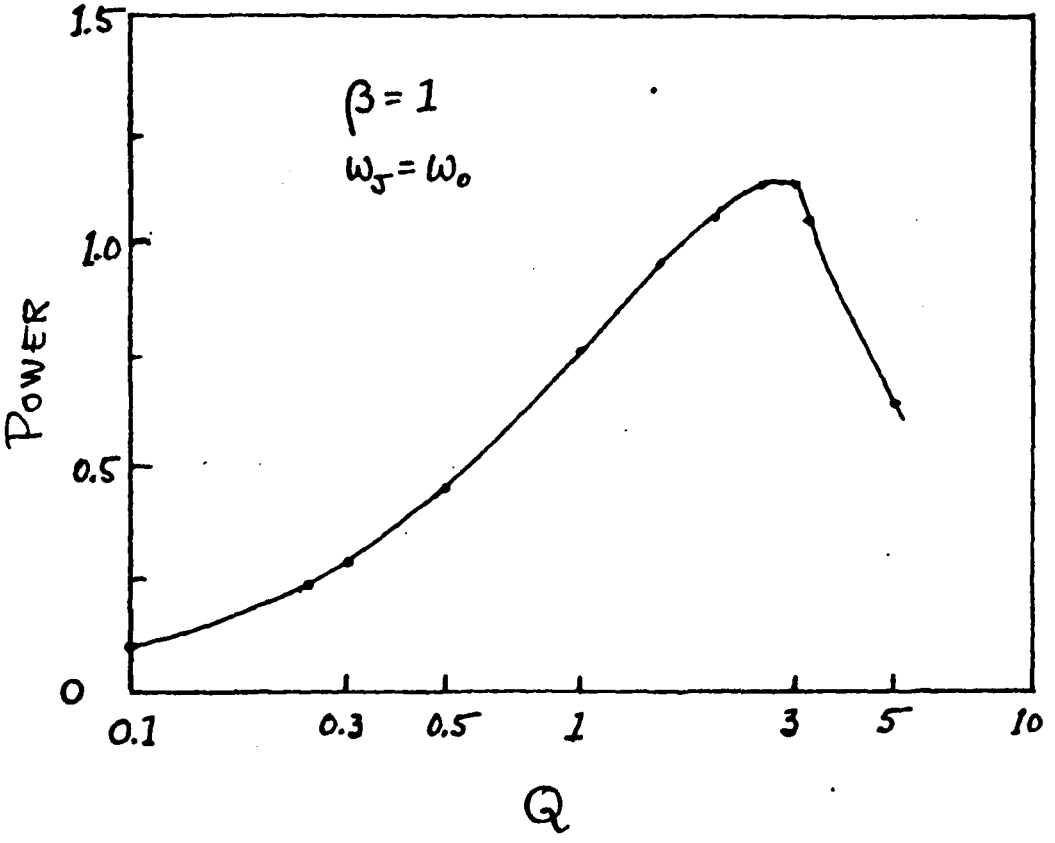

FIGURE 6. Computed power delivered to the load resistance R in the resistive SQUID at ω_J as a function of the loaded Q. Power is in units of $[\omega_o \phi_o^2/(2\pi)^2 L]$.

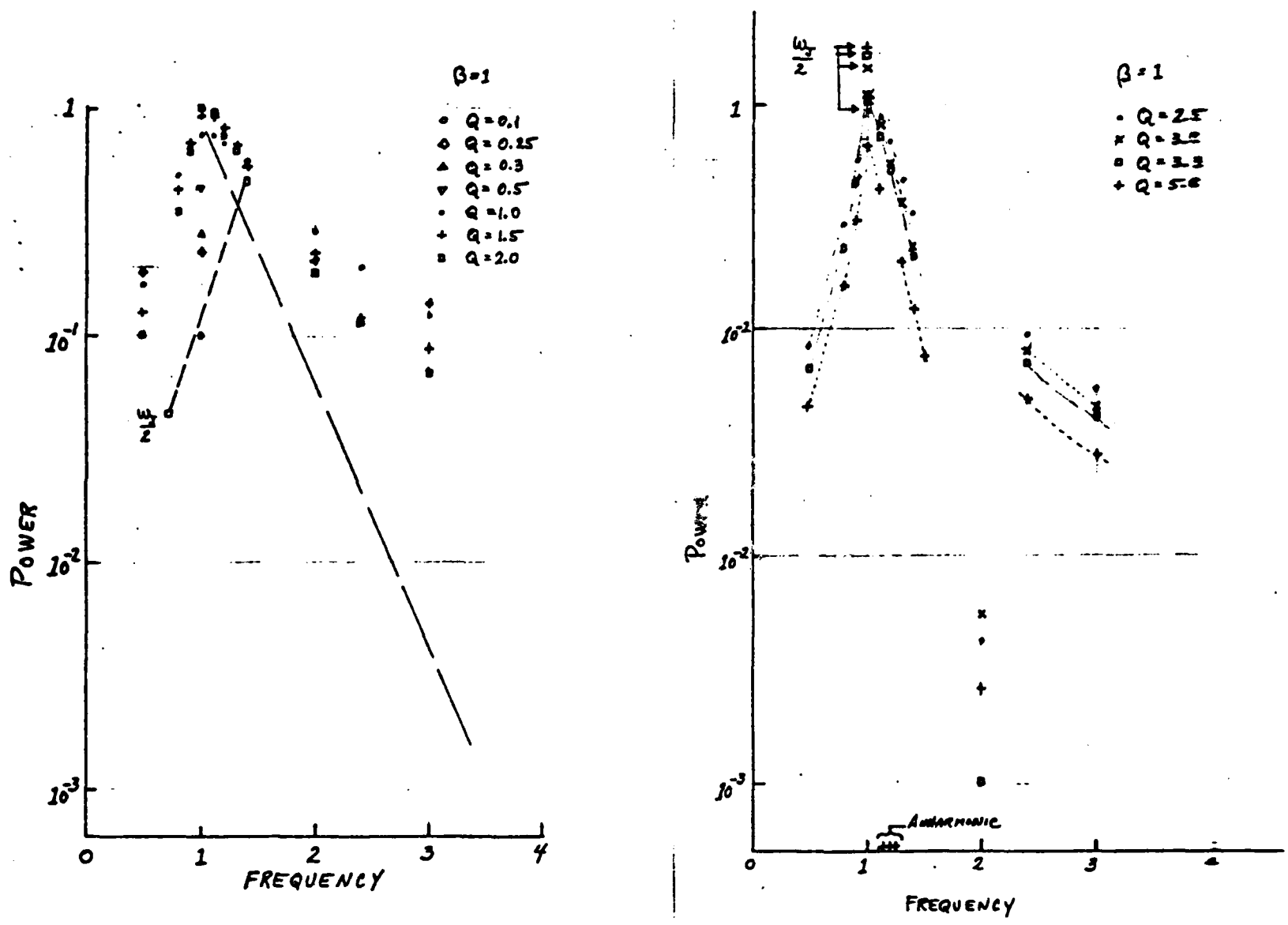

FIGURE 7. Computed power delivered to the load resistance in the resistive SQUID as a function of the Josephson frequency for various values of Q with β=1. Power is normalized by $[\omega_o \phi_o^2/(2\pi)^2 L]$ and frequency by ω_o.

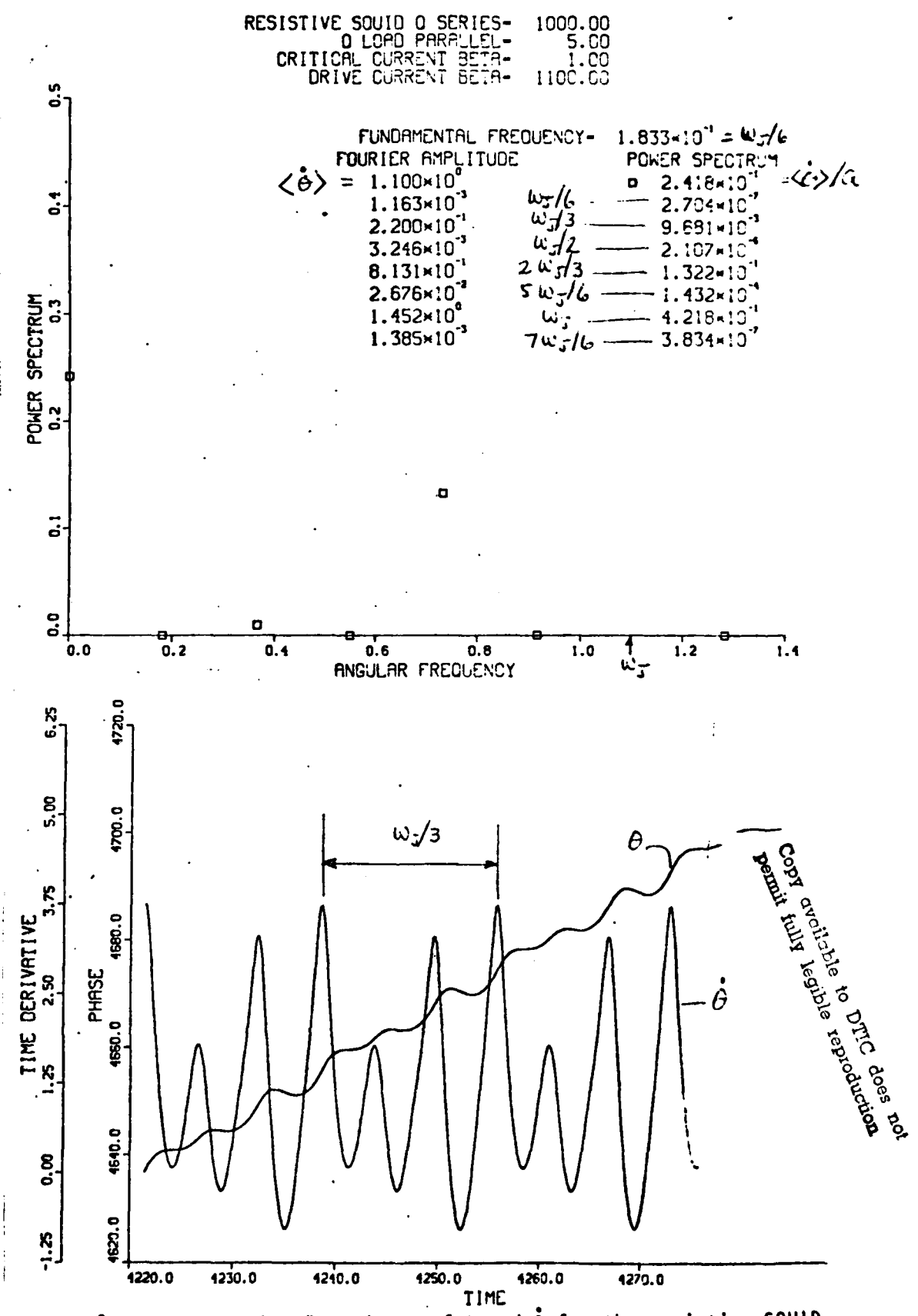

FIGURE 8. Computed time dependence of θ and $\dot{\theta}$ for the resistive SQUID (lower graph) and power spectrum (upper graph) for Q=5, β=1 and β_l=1100, corresponding to ω_J=1.1ω_o. Time is measured in ω_o^{-1} and frequency in ω_o.

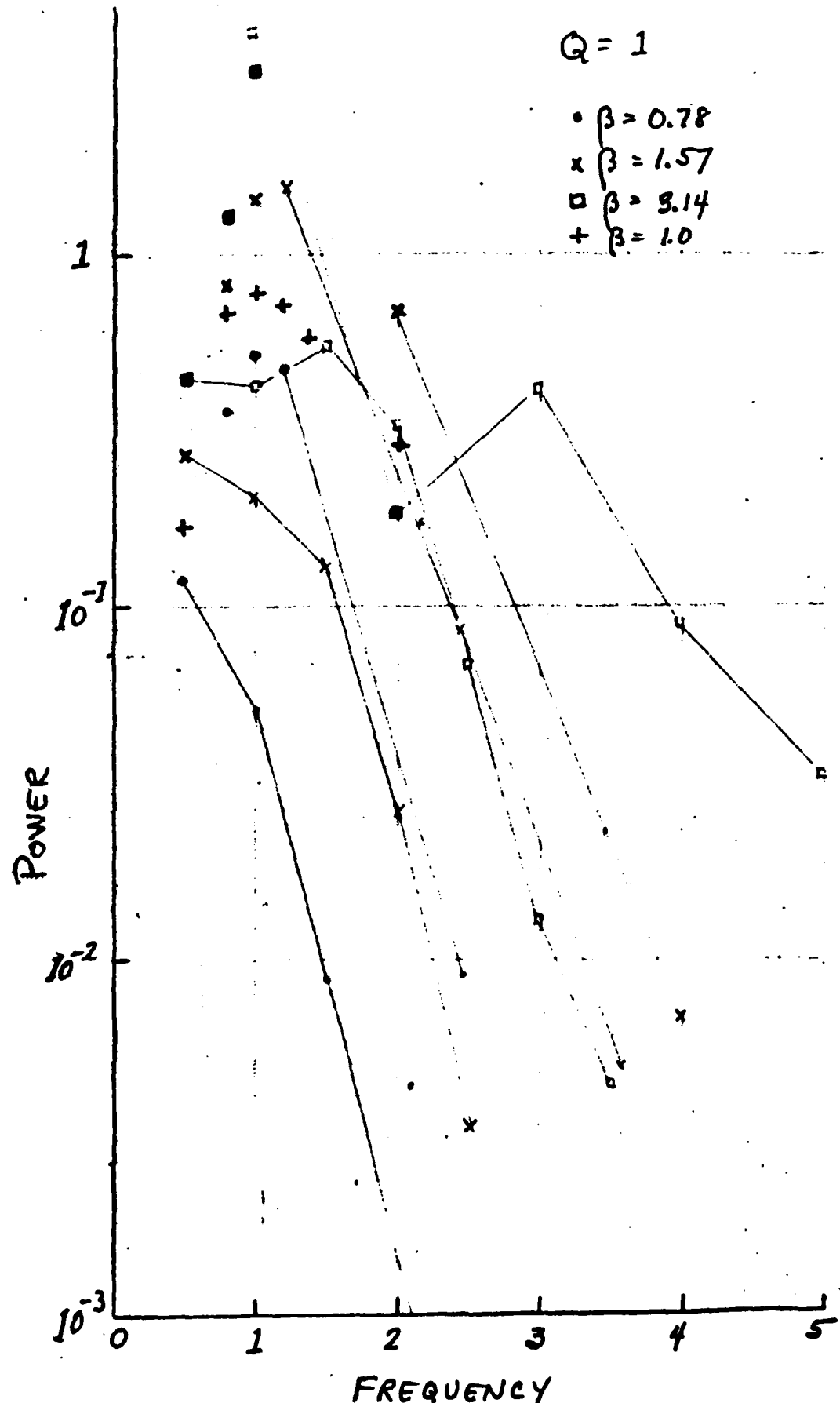

FIGURE 9. Computed power delivered to the load resistance in the resistive SQUID with Q=1 as a function of β. Power is measured in $[\omega_e \phi_e^2/(2\pi)^2 L]$ and frequency in ω_e.

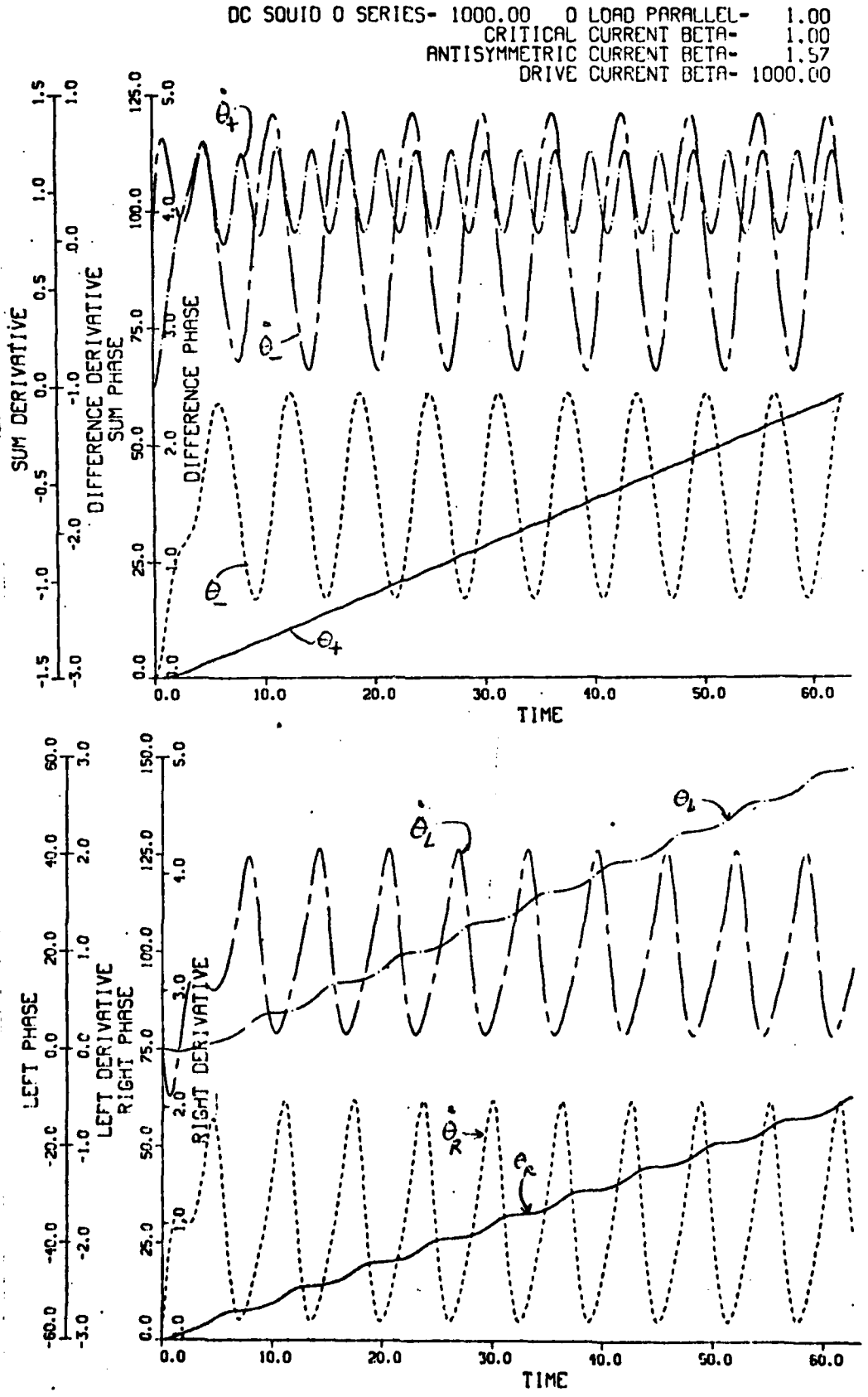

FIGURE 10. Time evolution of the phases and their time derivative in the voltage-clamped dc SQUID with Q=1, β=1, β_l=1.57 and $\omega_J \simeq \omega_o$. Time is measured in ω_o^{-1}.

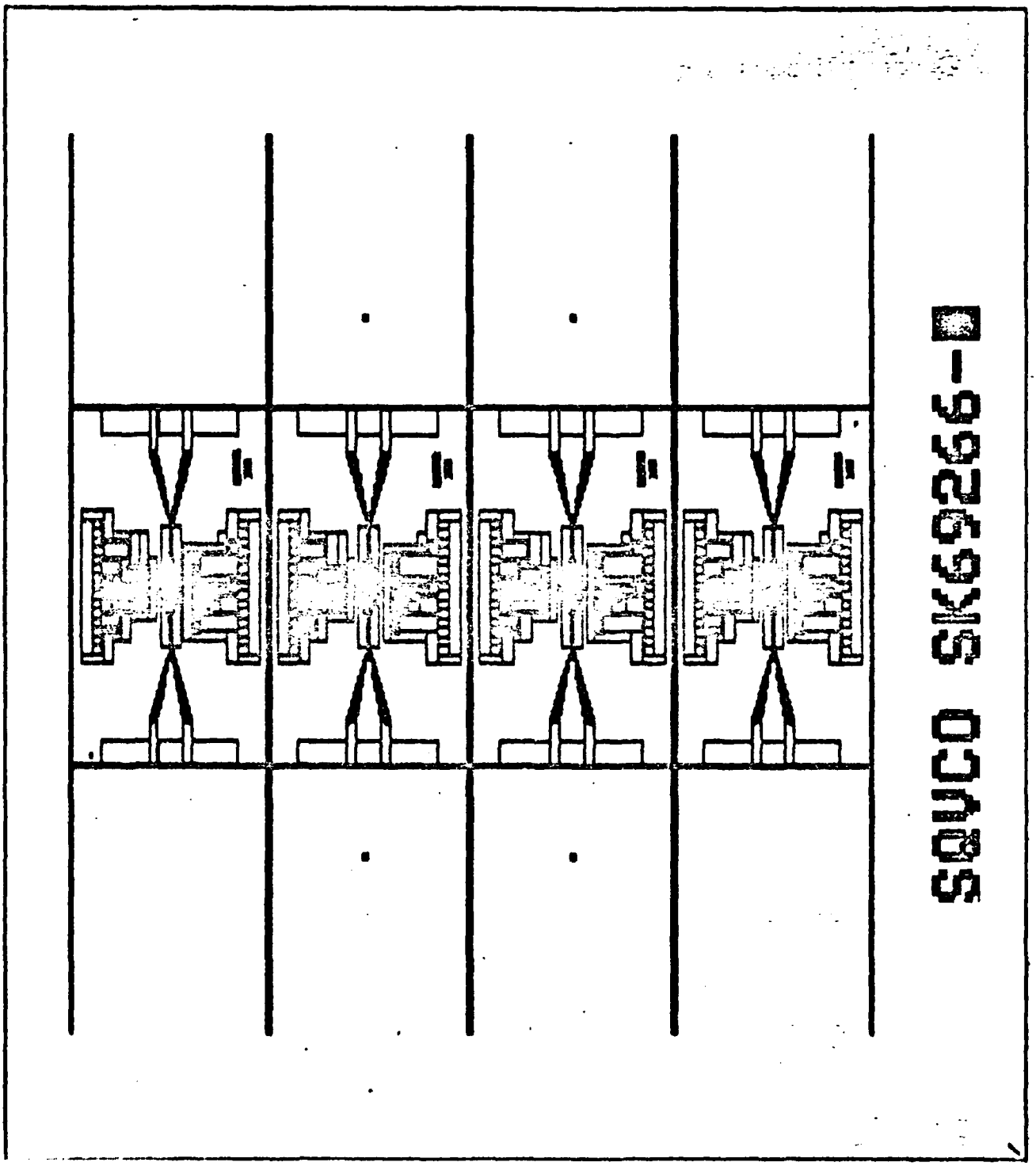

FIGURE 11. Composite of seven masks designed for the four VCO circuits. Test junctions and resistors are placed above and below each of the 2 VCO's per chip.

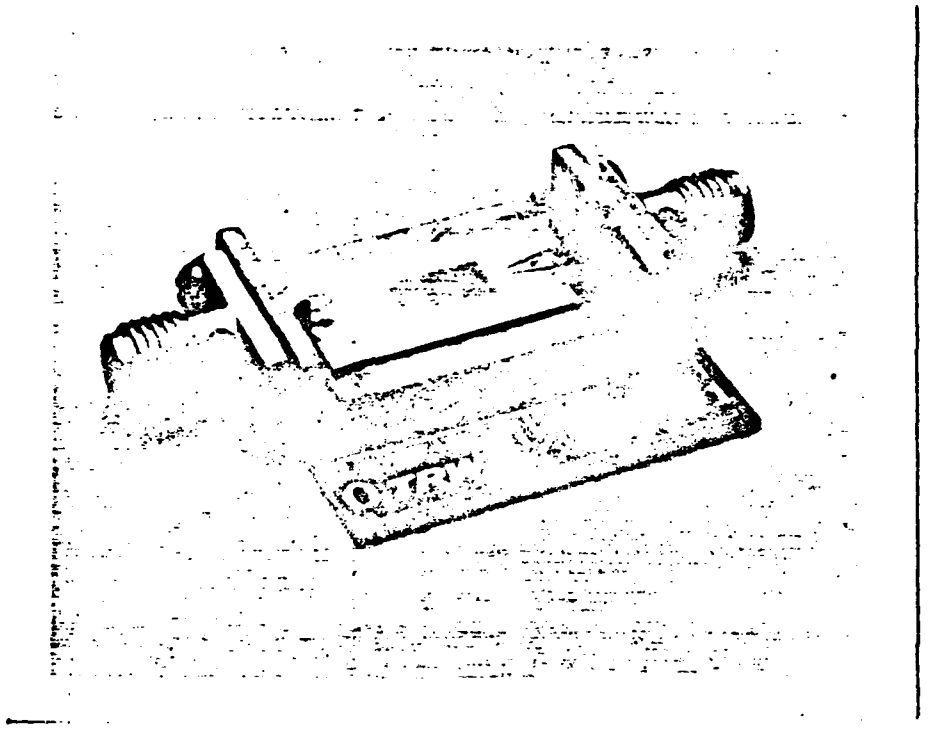

Figure 12. Photograph of transformer test chip mounted in a brass holder and connected to two OSM bulkhead connectors. The tapered coplanar lines at each end are visible in the photograph. The grey rectangle in the center of the chip is anodized Nb covered with SiO. The transformers are located in the same rectangle but are not clearly visible in the photograph.

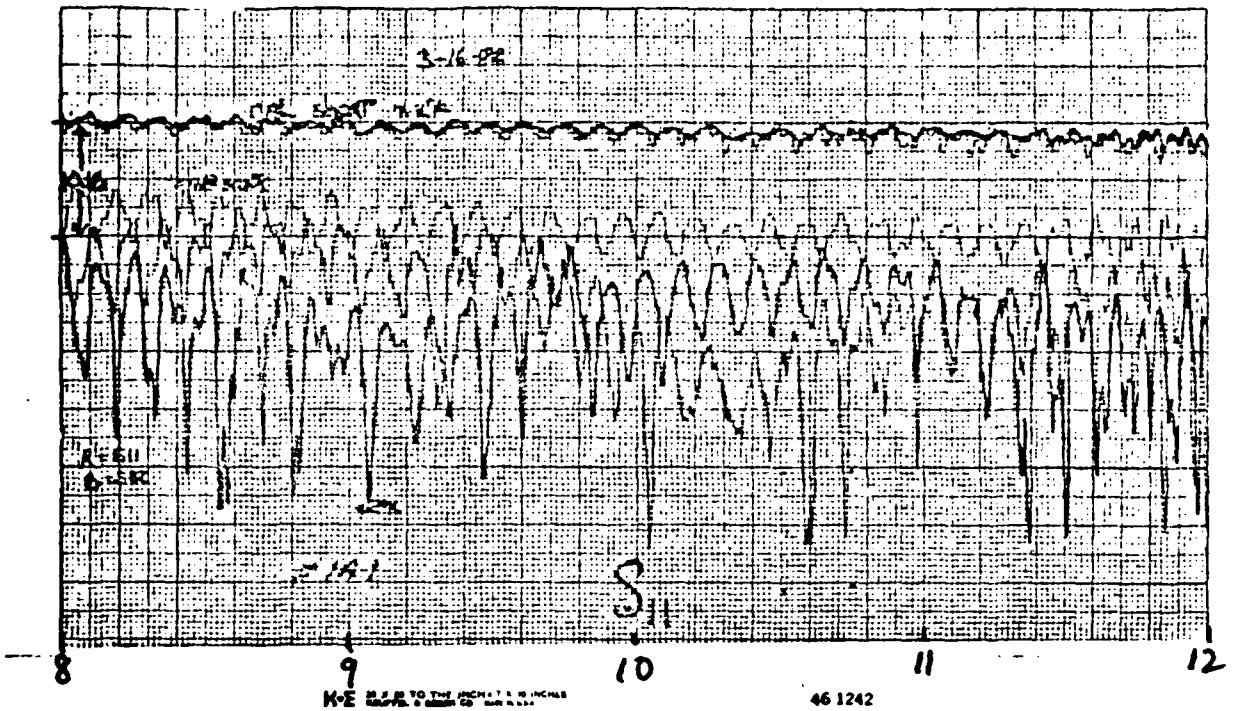

K-E 46 1242

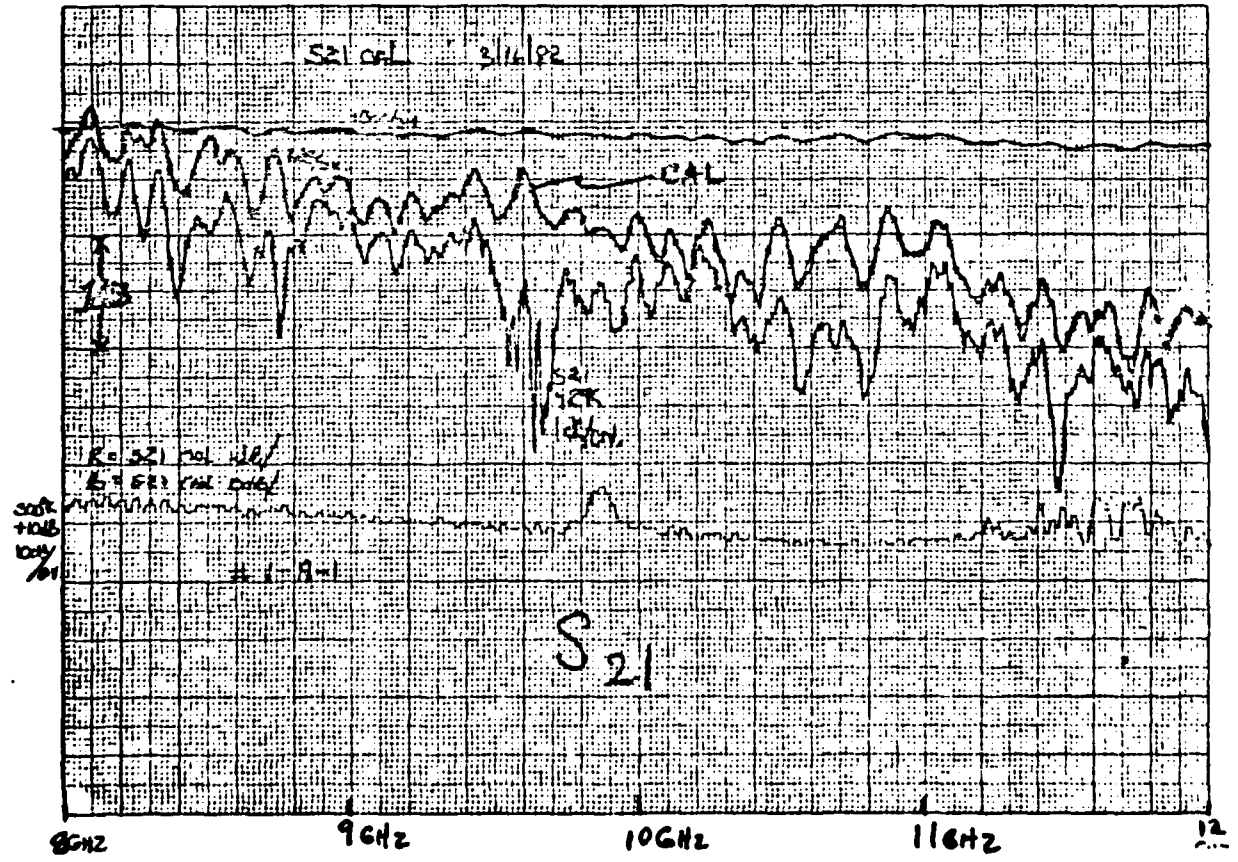

Figure 13. Response of 50Ω tapered coaxial lines on silicon substrate measured at 4K. The upper graph shows S_{11} (and S_{22}) at 4K; the faint curve is S_{11} at 300K. The lower graph is S_{21} at 4K.

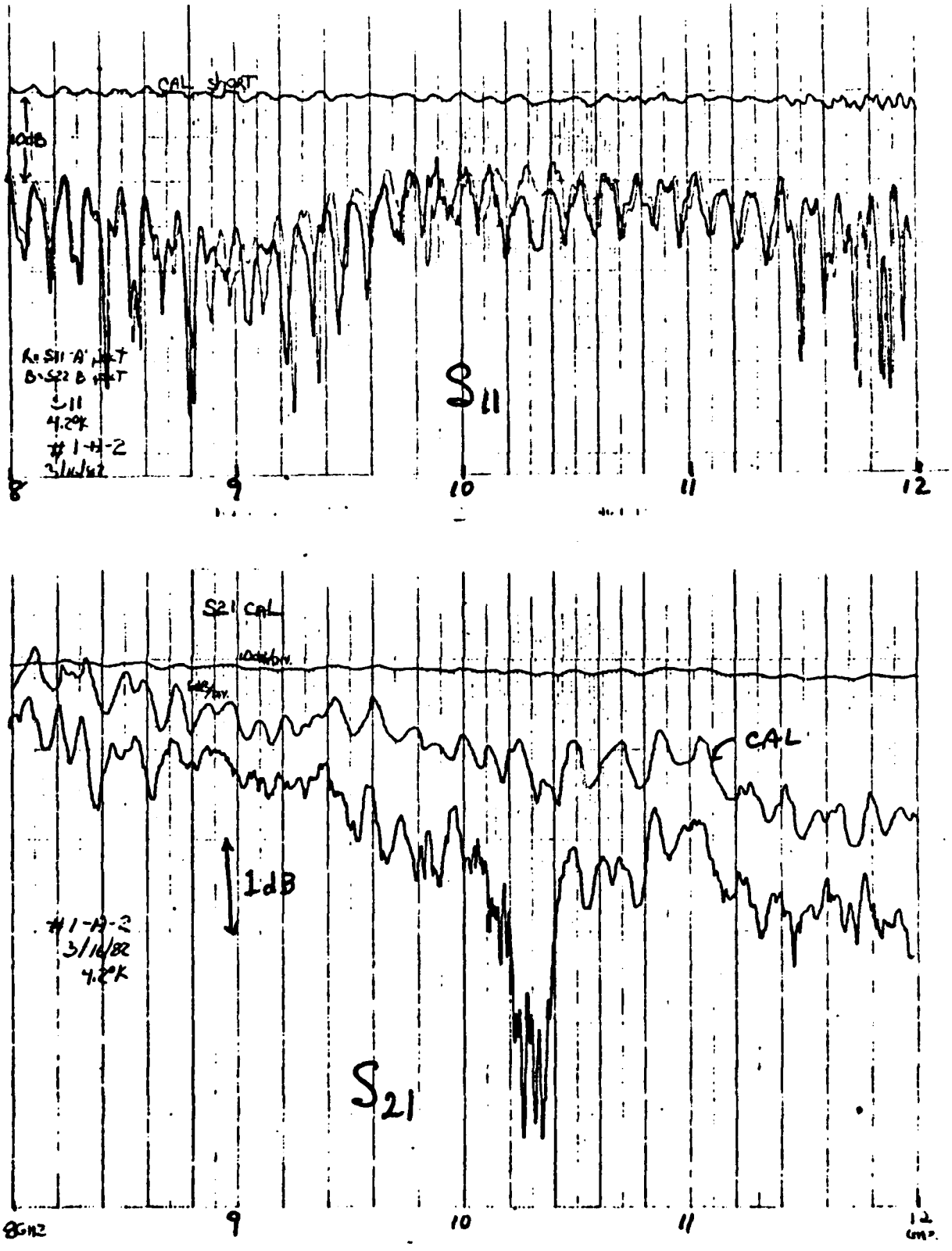

Figure 14. Response of the double-ended 50Ω to 1Ω transformers measured at 4K. The upper graph is S_{11} (and S_{22}), the lower is S_{21}.

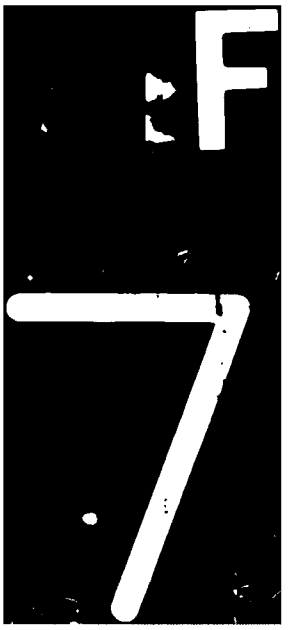
F
7